

On low-frequency waves in the surf and swash

Harshinie Karunarathna*, Andrew J. Chadwick

School of Engineering, Reynolds Building, University of Plymouth, Drake Circus, Plymouth PL4 8AA, UK

Received 17 October 2006; accepted 15 May 2007

Available online 25 May 2007

Abstract

Low-frequency waves in the surf and swash zones on various beach slopes are discussed using numerical simulations. Simulated surface elevations of both primary waves and low-frequency waves across the surf zone were first compared with experimental data and good agreement found. Low-frequency wave characteristics are then discussed in terms of their physical nature and their relationship to the primary wave field on a series of sea bottom slopes. Unlike primary waves, low-frequency wave energy increases towards the shoreline. Low-frequency waves in the surf and swash are a function of incident waves and the sea bottom slope and hence the saturation level of the surf zone. Wave energy on a gently sloping beach is dominated by low-frequency waves while primary waves play a significant role on a steep beach. Low-frequency wave radiation from the surf zone on a given beach depends on primary wave frequency and beach slope. However, a very poor correlation was found between surf similarity parameter and low-frequency wave radiation.

© 2007 Published by Elsevier Ltd.

Keywords: Low frequency waves; Surf zone; Bichromatic wave groups; Wave groupiness; Bound low-frequency wave; Break point generated long wave; Swash oscillation

1. Introduction

The presence of low-frequency waves in the surf and swash regions is well established in the literature through a vast number of field investigations and laboratory measurements. Low-frequency waves play a very significant role in water surface fluctuations and sediment mobility in the surf and swash zones. Therefore, it is extremely important to quantify them in understanding the evolution of near-shore morphology and in the design of sea defence and other coastal structures.

Low-frequency waves were first observed outside the surf zone by Munk (1949). He suggested that they were caused by the variability of mass transport by the incident waves and named them as surf beat. Tucker (1950) cross-correlated the incident short wave envelope and the low-frequency wave. He found that there was a negative peak in the cross-correlation function at a lag approximately corresponding to the time required for the short wave to travel to the shore and a low-frequency wave to return.

After the pioneering research by Munk (1949) and Tucker (1950), a large number of field investigations established the significance of low-frequency wave motions in the near-shore zone (Huntley et al., 1981; Guza and Thornton, 1985).

Following these observations, Longuet-Higgins and Stewart (1962, 1964) proposed that the low-frequency waves were generated due to non-linearity of the primary waves and remain bound to the primary wave groups. They also suggested that surf beat was consistent with the release of this bound wave during breaking of primary waves and subsequent reflection from the shoreline.

Symonds et al. (1982) proposed a model for low-frequency wave generation due to the time-varying breakpoint of primary waves. According to their theory, resulting low-frequency wave height is proportional to the height of incident primary waves. This model proposed that the low-frequency wave generated due to time-varying breakpoint radiates both seaward and shoreward. The shoreward propagating low-frequency wave subsequently reflects at the shoreline.

Schäffer (1993) developed a theory describing low-frequency wave generation in the near-shore. He identified

*Corresponding author. Fax: +44 01752 233658.

E-mail address: gkarunarathna@plymouth.ac.uk (H. Karunarathna).

Nomenclature			
B	frequency dispersion parameter	L_0	deepwater wave length
f	incident wave frequency	P	volume flux
f_m	mean frequency of bichromatic wave groups	R	surface roller of breaking waves
g	acceleration due to gravity	R_c	radiation coefficient
GF	wave group factor	s	beach slope
GF ₀	wave group factor at offshore	$S(f)$	wave spectrum
h	still water depth	t	time
h_c	water depth at which the slot begins	x	distance offshore from still water line
H_0	deepwater wave height	δ	relative slot width w.r.t. unit beach width
H_s	significant wave height of short waves	Δf	frequency interval of bichromatic wave groups
H_1	low-frequency wave height	η	surface elevation
$(H_{lsw})_{max}$	maximum low-frequency swash excursion	η_{sw}	vertical elevation of swash
		λ	shape parameter
		ξ	surf similarity parameter

three causes of low-frequency wave generation; forcing outside the surf zone, time variation of the wave break point and transmission of the remaining wave groupiness in the surf zone.

Baldock et al. (1999) and Baldock and Huntley (2002) measured time-varying breakpoint generated low-frequency waves using bichromatic wave groups and random waves in a wave flume and confirmed that the generation of low-frequency waves depends on the normalised width of the surf zone as suggested by Symonds et al. (1982). They confirmed that the low-frequency wave generation is dependent on the normalised width of the surf zone as suggested by Symonds et al. (1982). Baldock and Huntley (2002) also found that the breakpoint variability in the surf zone as the dominant forcing mechanism of generating low-frequency waves from steep incident short waves.

Karunarathna and Tanimoto (1995,1996) discussed low-frequency waves on coastal shelves with a steep seaward face. They found substantial water surface fluctuations on coastal shelves at the frequency of primary waves. Karunarathna et al. (2005) discussed low-frequency waves in the swash and found that swash motions on gentle slopes are dominated by low frequency waves.

Primary wind or swell waves are transformed into a range of low-frequency waves due to wave breaking, the variability of break point within the surf zone and the variation of sea bottom bathymetry. Since the short wave breaking is strongly influenced by the sea bottom bathymetry, low-frequency waves on mild sandy beaches are expected to be significantly different from those on steep shingle or mixed beaches.

This paper discusses low-frequency waves in the surf and swash regions on a variety of plane beaches covering mild to steep sea bottom slopes. The discussion is based on numerically derived results of low-frequency waves. The relationship between low-frequency waves and dissipation of primary waves together with the evolution of incident wave groupiness in the near-shore is also investigated. The numerical model used in the present study is first validated against experimental data on primary water surface

elevations in the surf and swash and then against experimentally derived data on low-frequency waves in the surf zone. Then, a series of numerical experiments was carried out to investigate low-frequency waves and their relationship with the incident primary wave field. The paper unifies the previous laboratory and field investigations and theoretical developments of low-frequency waves in the surf and swash zones.

Section 2 of the paper gives a brief description of the numerical model used in the present study with the boundary conditions. In Section 3, the validation of the model against experimental data is presented. Section 4 gives results and discussion of numerical experiments. Section 5 draws conclusions based on the findings from the results shown in Section 4.

2. Numerical model

2.1. Governing equations

The numerical wave model used in the present study solves the weakly non-linear 1D Boussinesq equations derived by Madsen et al. (1991, 1997a, b) with a surface roller to accommodate wave breaking and dissipation. The governing equations of continuity and conservation of momentum flux in terms of surface elevation η and volume flux P are given by

$$\gamma(\eta) \frac{\partial \eta}{\partial t} + \frac{\partial P}{\partial x} = 0, \quad (1)$$

$$\begin{aligned} \frac{\partial P}{\partial t} + \frac{\partial}{\partial x} \left(\frac{P^2}{A} \right) + \frac{\partial R}{\partial x} + gA \frac{\partial \eta}{\partial x} \\ = \left(\frac{1}{3} + B \right) h^2 \frac{\partial^3 P}{\partial x^2 \partial t} + Bgh^3 \frac{\partial^3 \eta}{\partial x^3} \\ + h \frac{\partial h}{\partial x} \left(\frac{1}{3} \frac{\partial^2 P}{\partial x \partial t} + 2Bgh \frac{\partial^2 \eta}{\partial x^2} \right), \end{aligned} \quad (2)$$

where R , is the surface roller, h the still water depth, B the frequency dispersion parameter and g the acceleration due

to gravity. Parameters γ and A , which are related to the shoreline boundary are described in Section 2.2.

2.2. Boundary conditions

The model uses an internal wave generation routine at the offshore boundary. Waves propagated seaward of the generation boundary are absorbed by a dissipating sponge layer. The thickness of the sponge layer exceeded twice the length of the longest wave generated for the simulations. The model is capable of generating solitary waves, cnoidal waves, regular waves, random waves with two defined energy spectra and fully or partially modulated bichromatic wave groups.

A moving shoreline is established at the shoreward boundary by using the ‘slot’ technique developed by Kennedy et al. (2000). The change in unit width of the beach due to the incorporation of a slot is parameterised by the $\gamma(\eta)$ and A in Eqs. (1) and (2) where

$$\gamma(\eta) = \begin{cases} 1, & \eta > z^*, \\ \delta + (1 - \delta)e^{\lambda/h_0(\eta - z^*)}, & \eta \leq z^*, \end{cases} \quad (3)$$

$$A = \begin{cases} (\eta - z^*) + \delta(z^* + h_0) + \frac{h_0(1 - \delta)}{\lambda}(1 - e^{-\lambda(1 + z^*/h_0)}), & \eta > z^*, \\ \delta(\eta + h_0) + \frac{h_0(1 - \delta)}{\lambda} \times (e^{\lambda/h_0(\eta - z^*)})(1 - e^{-\lambda(1 + z^*/h_0)}), & \eta \leq z^*, \end{cases} \quad (4)$$

$$z^* = \frac{-h}{1 - \delta} + h_0 \left(\frac{\delta}{1 - \delta} + \frac{1}{\lambda} \right), \quad (5)$$

where δ is the relative width of the slot with respect to the unit width of the beach, λ is the shape parameter which controls the smooth transition of cross-sectional area from unit width of the beach to narrow slot. h_0 is the water depth where the slot begins.

The full description of the numerical wave model, selection criterion of suitable slot parameters, numerical stability of the model and a sensitivity analysis of slot parameters are given in Karunarathna et al. (2005).

2.3. Numerical wave channel

Numerical simulations were carried out in a numerical wave flume shown in Fig. 1. For the results discussed in

Section 3 (except simulations used for model validation), offshore water depth was maintained at 1.0 m. Numerical simulations were carried out on three different plane beaches with 1:10, 1:20 and 1:30 slopes, covering a wide spectrum of natural beaches including shingle, mixed grain and sand beaches. A horizontal sea bed of 10 m was maintained between the internal wave generation boundary and the foot of each slope. The beach slope extended up to 0.2 m above the still water shoreline and then followed by a 2.0 m wide horizontal section. Sponge layers, which were two wave lengths wide, were incorporated at both offshore and shoreline boundaries to dissipate wave energy propagating offshore and wave energy propagating through the slot. The spatial resolution of the computations was 0.05 m while the time step was 0.01 s.

3. Model validation

Model performance regarding propagation of short wave groups on various beach slopes is given in Karunarathna et al. (2005). Primarily, the model results are compared with two sets of experimental data of regular waves and bichromatic wave groups. The first set of data, which was collected by Mase (1994, 1995) covers bichromatic wave groups propagating across a 1:20 beach. The incident bichromatic waves were fully modulated. Bichromatic wave groups with two different energy levels and three different frequencies covering six wave cases were considered for comparison. The second set of data was collected at Imperial College (Baldoock et al., 1997). The measurements were carried out on a 1:10 beach slope. The entire set of data contains two cases of regular waves, two cases of bichromatic groups and two cases of irregular waves.

Fig. 2 compares numerical predictions with Mase’s (1994, 1995) experimental data at three different water depths along the channel. Measured surface elevations of primary wave groups (η) in the surf zone and associated swash excursions are compared with numerical results. The incident waves were fully modulated bichromatic groups with a primary frequency $f = 0.6$ Hz and a frequency interval $\Delta f = 0.06$ Hz. Waves propagated at a 0.47 m water depth before reaching the 1:20 beach slope. The simulated results are in very good agreement with the measured data. Further comparisons and root mean square errors of numerical results can be found in Karunarathna et al.

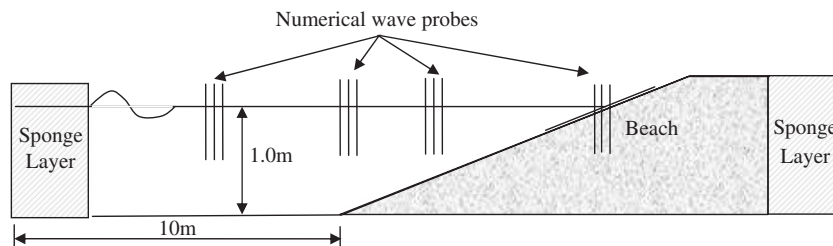


Fig. 1. Numerical wave channel.

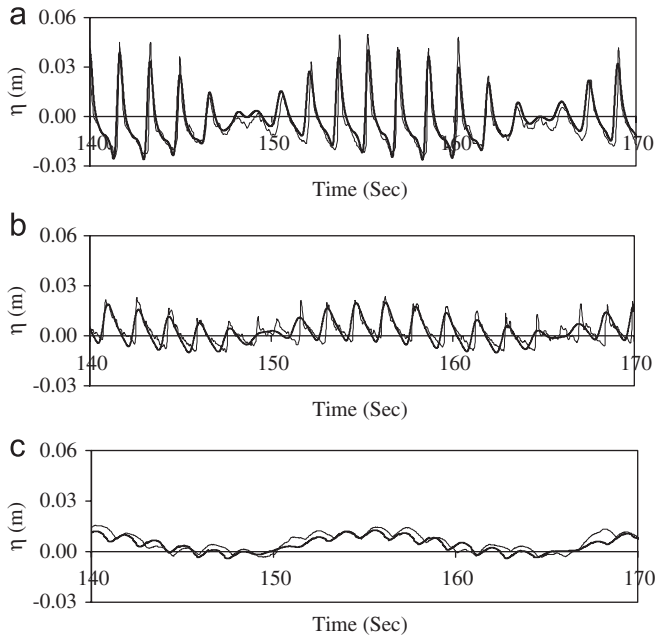


Fig. 2. Comparison of measured and simulated surface elevation in the surf zone and swash. $f_m = 0.6$ Hz, $\Delta f = 0.06$ Hz. (a) $h = 7.5$ cm, (b) 2.5 cm, (c) vertical swash excursion. Dark line—simulated, faint line—measured (Mase, 1995).

(2005). It can be seen that the model predicted surface elevations of primary waves in the surf zone and swash excursions with less than 11% root mean square error.

The spatial distributions of simulated low-frequency wave amplitudes on a 1:20 sea bottom slope were then compared with experimentally derived low-frequency waves. The experimental results were from Mase (1995). This data contained surface elevations measured across the surf zone at 12 locations with surface piercing wave gauges and swash oscillations measured using a run-up meter. The incident bichromatic waves were fully modulated. Offshore water depth was kept at 0.47 m and the experimental setup had a 10 m long region of constant water depth prior to the commencement of the slope. The experiments covered a range of incident wave groups with various primary wave frequencies, frequency intervals and wave heights. The fast Fourier transform (FFT) had been used to analyse surface elevation time series containing 2048 data points with a 40 Hz sampling frequency to derive low-frequency wave amplitudes from the surface elevations of the primary waves. The normalised low-frequency wave amplitudes were then computed as $\sqrt{S(f_{\max})}/\sqrt{S_s(f_{\max})}$, where $S(f_{\max})$ is the energy density of the low-frequency wave, $S_s(f_{\max})$ is the energy density of the corresponding swash oscillation and f_{\max} is the measured peak frequency of the swash oscillations.

Figs. 3 and 4 present comparisons of the experimentally derived and numerically reproduced spatial distribution of normalised low-frequency wave amplitudes for the following two wave cases: Case (A)—bichromatic wave groups with primary frequency $f = 0.6$ Hz and frequency interval $\Delta f = 0.1$ Hz and Case (B)—bichromatic wave groups with

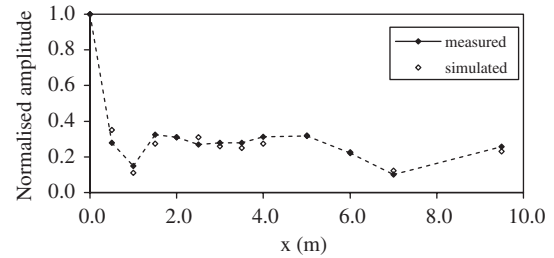


Fig. 3. Low-frequency wave across the surf zone. $f = 0.6$ Hz and frequency interval $\Delta f = 0.1$ Hz. Dark line—simulated, faint line—measured (Mase, 1995).

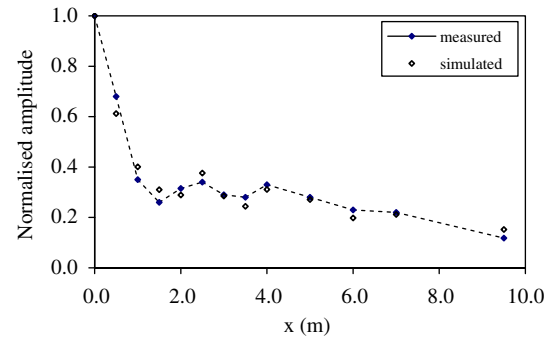


Fig. 4. Low-frequency wave across the surf zone. $f = 0.6$ Hz and frequency interval $\Delta f = 0.05$ Hz. Dark line—simulated, faint line—measured (Mase, 1995).

primary frequency $f = 0.6$ Hz and frequency interval $\Delta f = 0.05$ Hz. The low-frequency wave amplitudes were normalised against the amplitude at the still water shoreline.

It can be seen in the above two figures that the model accurately reproduces the low-frequency waves. The average root mean square error of low-frequency wave amplitude $[\frac{(\eta_1^S - \eta_1^M)^2}{(\eta_1^M)^2}]^{1/2}$, where η_1^S and η_1^M are simulated and measured low-frequency wave amplitude, respectively] across the surf zone for Cases (A) and (B) were 11% and 10%, respectively, which indicates that the model reproduces low-frequency waves with good accuracy.

4. Results and discussion

This section of the paper presents the results and discusses low-frequency waves in the surf and swash zones on various different sea bottom slopes. The incident primary waves used in this study were fully modulated bichromatic wave groups with closely spaced frequency components. The resulting wave groups have an envelope modulated at a frequency equal to the frequency spacing of the component waves. Table 1 lists the bichromatic wave groups used for the following discussions. The amplitude of each primary wave component was kept at a constant value of 0.05 m for all cases presented in this paper. The incident wave conditions were carefully selected to cover spilling to surging type wave breakers. Table 2 shows surf similarity parameters (ξ) of the incident waves.

Table 1
Incident bichromatic wave groups used for discussion

Wave case	Mean frequency f (Hz)	Δf (Hz)
1	0.4	0.04
2	0.6	0.06
3	0.8	0.08

Table 2
Surf similarity parameters of incident waves

f (Hz)	H_0/L_0	ζ at 1:10	ζ at 1:20	ζ at 1:30
0.4	0.010	1.00	0.50	0.333
0.6	0.023	0.659	0.329	0.220
0.8	0.041	0.479	0.494	0.164

Low-frequency waves were calculated on 1:10, 1:20 and 1:30 beach slopes using the FFT technique and band-pass filtering of the simulated surface elevation time series of the primary wave groups. All surface elevation time series used in the present study contained 4096 data points sampled at a 100 Hz frequency interval.

Fig. 5 shows the numerical results of the spatial distribution of primary short wave heights (H_s) across the surf zone for all wave cases given in Table 1. Note that (a), (b) and (c) correspond to beach slopes 1:10, 1:20 and 1:30, respectively. The furthest offshore location of the depth limited wave breaking point is pushed towards the still water shoreline with increasing sea bottom slope. The outer breaking point of the primary waves varied between 8.0 and 1.5 m from the still water shoreline. The amount of short wave energy left at the still water shoreline varies considerably with the bottom slope where steep slopes with narrow surf zones possess higher wave energy near the shoreline.

Fig. 6 shows cross-shore variation of total low-frequency wave height (H_l) corresponding to the primary waves shown in Fig. 5. Low-frequency waves were derived in a finite frequency band within ± 0.01 Hz of the mean frequency of the primary waves. In the inner surf zone between the wave breaking point and the beach, low-frequency wave energy is mainly comprised two components: low-frequency wave energy generated due to the time-varying wave breaking point and the bound low-frequency wave energy. The dominance of one over the other depends on the intensity of wave breaking and the remaining groupiness of the primary waves in the inner surf zone. As opposed to the primary wave energy, low-frequency wave energy increases across the surf zone towards the still water shoreline. In some cases, low-frequency wave energy at the still water shoreline reached as high as 12 times its offshore counterpart. A general trend of increasing low-frequency wave energy at the still water shoreline was found with the decreasing sea bottom slope. On gentle slopes, the time-varying breakpoint

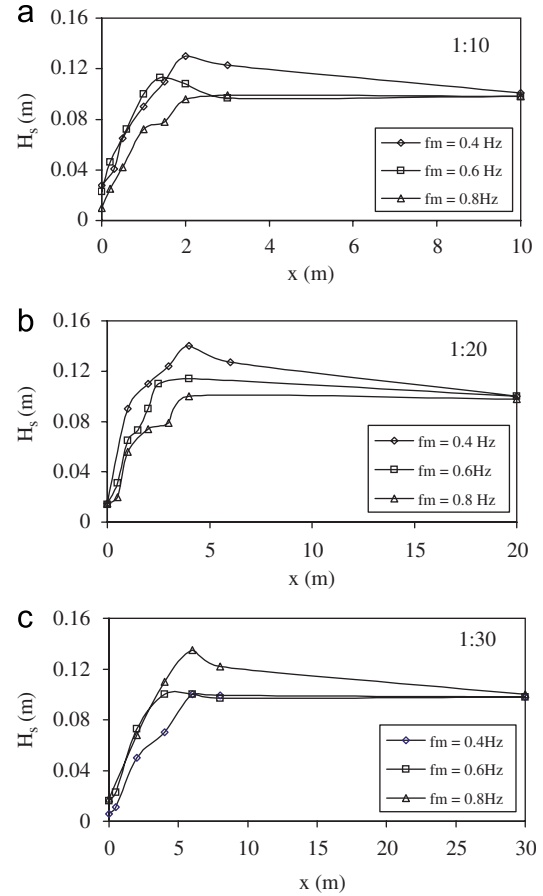


Fig. 5. Cross-shore variation of primary wave height. (a) $s = 1:30$, (b) $s = 1:20$, (c) $s = 1:10$.

generated low-frequency waves dominate due to the high intensity of wave breaking and the presence of a wide surf zone. It can also be seen that the low-frequency wave energy near the beach depends on the mean frequency of primary wave groups. Higher low-frequency wave energy was observed at lower primary wave frequencies.

Fig. 7 shows the cross-shore variation of wave height ratios of low-frequency and primary waves (H_l/H_s). It can be seen that the height of low-frequency waves in the inner surf zone is larger than that of the local primary waves except on the 1:10 beach where a significant proportion of the primary wave energy is preserved in the inner surf zone. The wave height ratio increases as beach slope becomes gentler. At the still water shoreline on the 1:30 slope, the low-frequency wave height could be more than 2.5 times the local primary wave height. This indicates the fact that the inner surf zone of a mild beach, where the surf zone is in near saturation, is driven mainly by the low-frequency wave energy. On the other hand, on steep beaches, where the surf zone is only partially saturated, both primary waves and low-frequency components have similar contributions to the surface fluctuations.

The low-frequency wave height distribution has a non-linear relationship with the height of depth limited primary

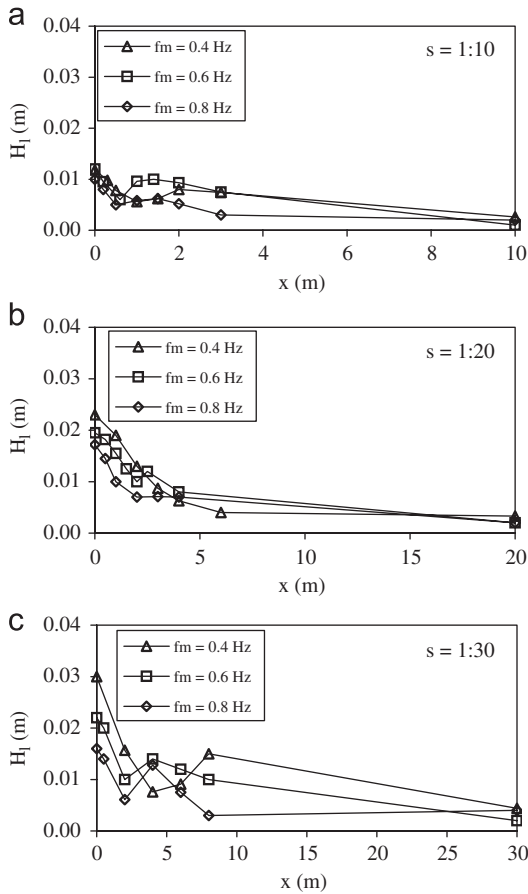


Fig. 6. Cross-shore variation of total low-frequency wave height. (a) $s = 1:30$, (b) $s = 1:20$, (c) $s = 1:10$.

waves in the inner surf zone. The wave group structure of the primary waves breaks down which leads to a dissipation of the bound low-frequency waves. Bound low-frequency waves maintain a non-linear relationship with primary waves at the offshore. With the dissipation of bound waves, low-frequency waves generated due to the time-varying break point begin to dominate the surf zone which shows a near linear relationship to the primary waves preserved in the surf zone. The local primary wave groupiness (GF) across the surf zone as a fraction of offshore wave groupiness (GF_0) is shown in Fig. 8 for a mean primary frequency of 0.6 Hz and for bottom slopes 1:30, 1:20 and 1:10. The height ratio of low-frequency and primary waves is also included in the figure for convenience of comparison.

Wave groupiness in the above figures is derived by the expression (List, 1991)

$$GF = \frac{\sqrt{2}\sigma_A}{\overline{A(t)}}, \quad (6)$$

where GF is the wave groupiness factor, σ_A and $\overline{A(t)}$ are the standard deviation and mean of the wave group envelop function derived from the surface elevation time series of primary wave groups. Surface elevation time series containing 4096 data points at a 200 Hz frequency interval

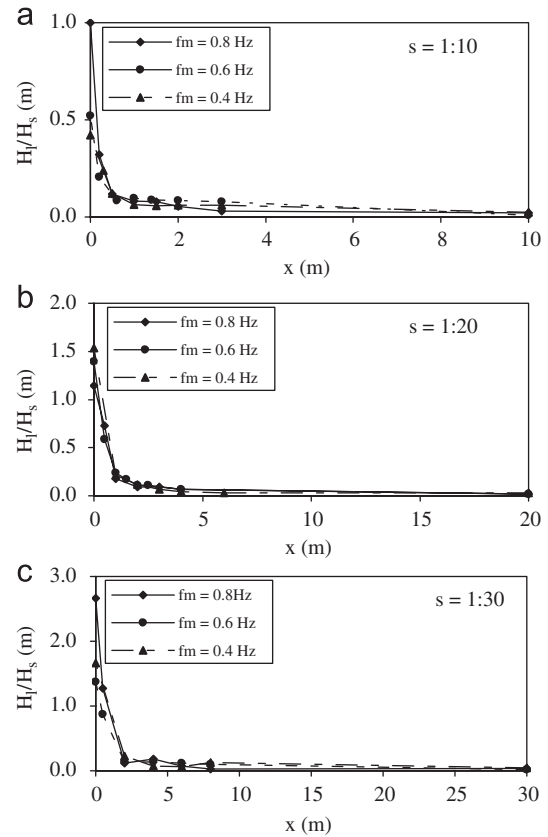


Fig. 7. Cross-shore variation of height ratio of total low-frequency wave and primary wave (H_1/H_s). (a) $s = 1:30$, (b) $s = 1:20$, (c) $s = 1:10$.

were used to derive wave groupiness. It can be seen in Fig. 8 that almost 75% of the primary wave groupiness is preserved at the still water shoreline of a 1:10 beach whereas not more than 30% of the groupiness remains at the same location on a 1:30 beach.

To confirm the relationship between primary wave groupiness and the low-frequency waves in the inner surf zone, wave energy spectra at the inner surf zone were then investigated. Fig. 9 shows the wave spectra ($s(f)$) at the still water shoreline on 1:30 and 1:10 beach slopes at the primary mean frequency of 0.6 Hz. In Fig. 9(a), very little primary wave energy remains at the still water shoreline of 1:30 slope. The low-frequency wave energy remaining at the same cross-shore location is an order of magnitude higher than that of primary waves. In contrast, on the 1:10 slope, the wave energies at both primary frequency and low-frequency are of the same order of magnitude.

The significance of low-frequency waves in driving swash excursions (η_{sw}) is seen in Fig. 10. Vertical swash displacement time histories on 1:30, 1:20 and 1:10 beach slopes are presented for $f = 0.6$ Hz and $\Delta f = 0.06$ Hz. As extensively discussed in Karunarathna et al. (2005), swash fluctuations on mild slopes are predominantly driven by wave energy at the frequency of the primary wave groups. On steep slopes, a significant proportion of short wave energy contributes to

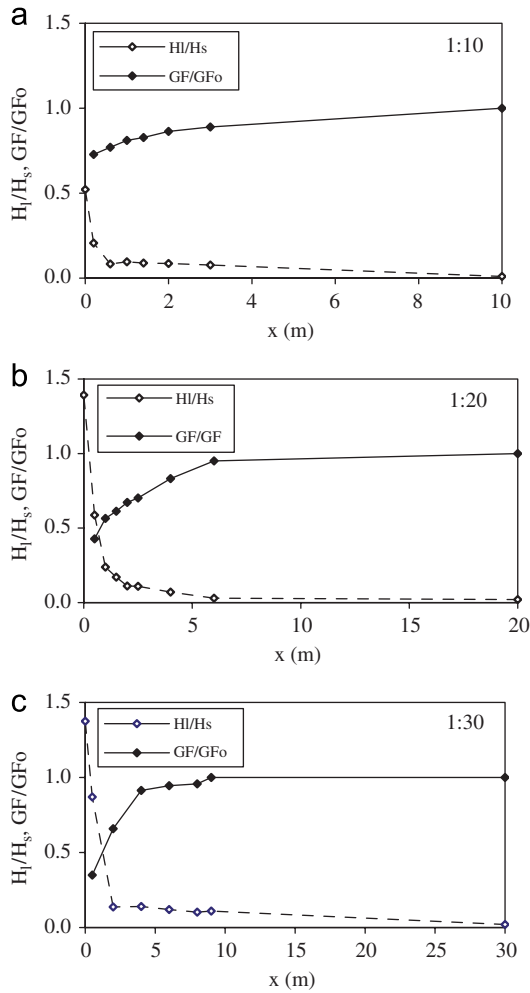


Fig. 8. Cross-shore variation of wave groupiness (GF) ($f_m = 0.6$ Hz). (a) $s = 1:30$, (b) $s = 1:20$, (c) $s = 1:10$.

drive swash motions and individual swash events driven by short waves become more significant.

The low-frequency component of swash was separated from the total swash signal by FFT and band-pass filtering. The maximum low-frequency swash excursion $[(H_{lsw})_{max}]$ against beach slope is plotted in Fig. 11. It can be seen that the low-frequency component of the swash excursion reduces with the increase in bottom slope irrespective of the mean frequency of the incident wave groups. The low-frequency component of the swash magnitude depends mainly on the breakpoint generated low-frequency wave and therefore, is related to the wave breaking mechanism and the width of the surf zone. Gentle slopes, where wave breaking point oscillates within a wide distance between the shoreline and the outer wave breaking point, generate higher low-frequency energy than that of steep slopes with narrow surf zones.

Low-frequency waves across the surf zone were then separated into incident and out-going components to investigate the radiation of low-frequency energy at wave breaking and reflection from the shoreline. The separation was carried out using the method presented by Baldock

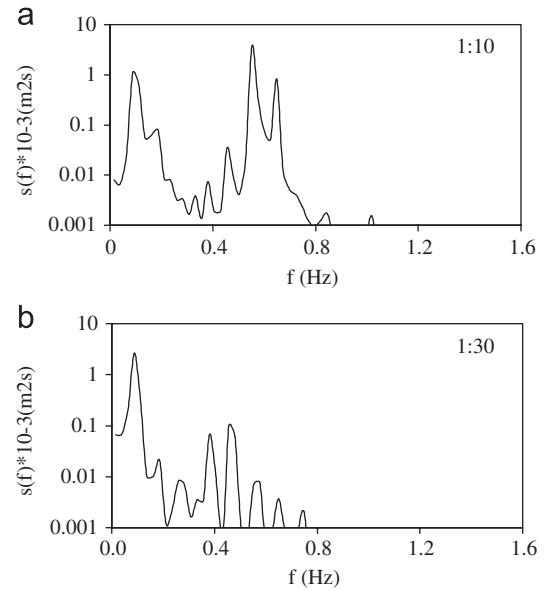


Fig. 9. Wave energy spectra at still water shoreline at $f_m = 0.6$ Hz, $\Delta f = 0.06$ Hz. (a) $s = 1:30$, (b) $s = 1:10$.

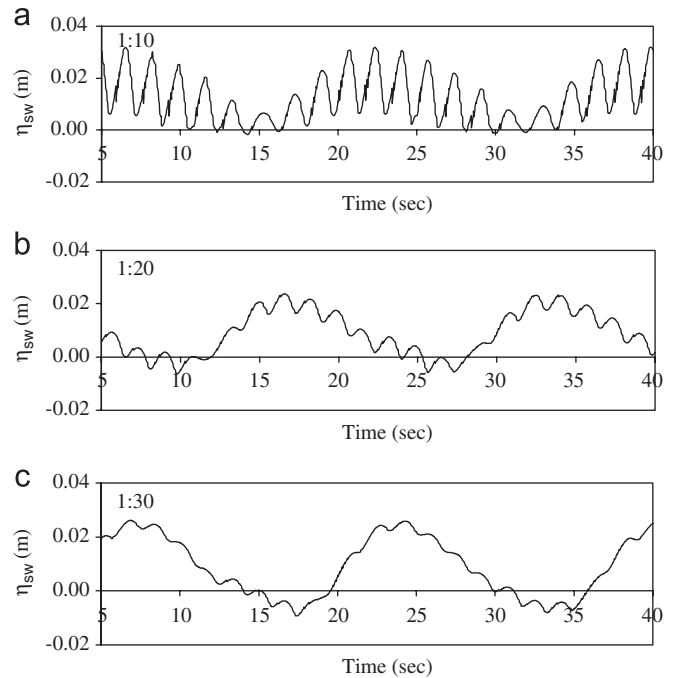


Fig. 10. Vertical swash displacement. $f_m = 0.6$ Hz, $\Delta f = 0.06$ Hz. (a) $s = 1:30$, (b) $s = 1:20$, (c) $s = 1:10$.

and Simmonds (1999). The method uses normally incident wave signals from spatially separated sensors over a sloping bottom.

Out-going free low-frequency waves are generated shoreward of the outer wave breaking point due to the time-varying wave breaking position in the surf zone and the change in bottom bathymetry. For fully modulated wave trains where the breaking zone extends up to the still water shoreline, radiated out-going low-frequency waves

can exist within the entire surf zone, irrespective of the reflection of low-frequency waves from the shoreline.

Fig. 12 shows the ratio of outgoing to incident low-frequency waves R_c (radiation coefficient, Baldock et al., 2002) for all three slopes considered in this paper (s1—1:30, s2—1:20 and s3—1:10). Low frequency wave amplitudes were obtained from the low-frequency wave energy spectra. The offshore value was calculated at the foot of the beach slope where the bottom slope meets the horizontal section of the numerical wave channel. It is seen that the value of R_c increases with increasing mean frequency of the primary wave groups. Higher frequencies lead to a wider surf zone where the position of wave breaking oscillates within a large distance, thus radiating a large proportion of low-frequency energy in both onshore and offshore directions.

In order to investigate the combined effect of beach slope and the incident wave conditions on low-frequency wave

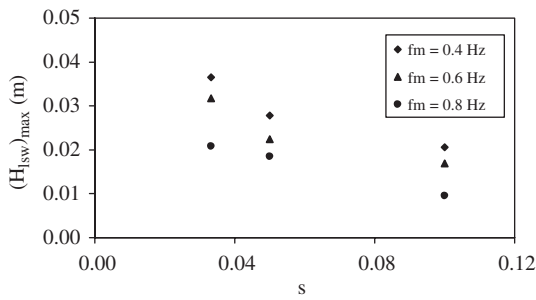


Fig. 11. Maximum low-frequency swash excursion against beach slope.

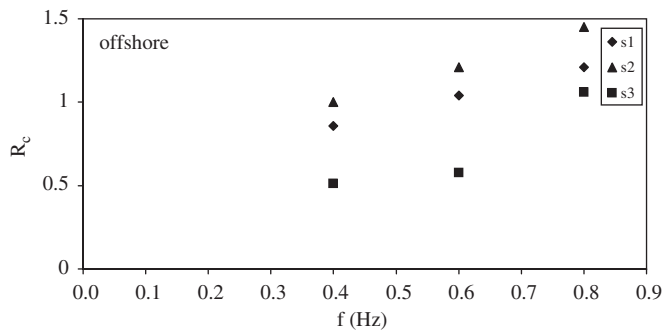


Fig. 12. Ratio of outgoing to incident low-frequency wave at the offshore against mean primary frequency.

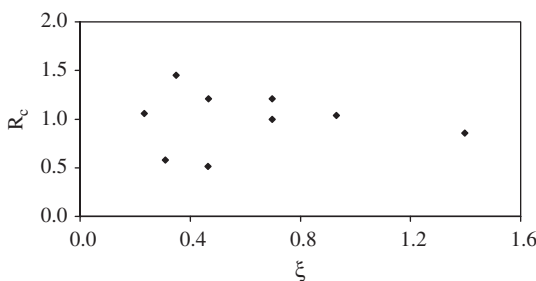


Fig. 13. Ratio of outgoing to incident low-frequency wave at the offshore against surf similarity parameter.

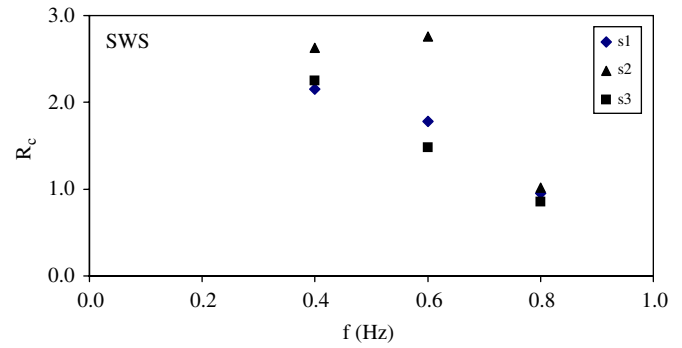


Fig. 14. Ratio of outgoing to incident low-frequency wave at the still water shoreline against mean primary frequency.

radiation, the radiation coefficient offshore is drawn against the surf similarity parameter $\xi = \tan \alpha / \sqrt{H_0/L_0}$ in Fig. 13. No apparent correlation is found between the two quantities. This indicates the fact that low-frequency waves maintain a complex relationship with primary wave conditions and beach slope.

The radiation coefficient (R_c) at the still water shoreline against mean frequency is shown in Fig. 14. A downward trend of R_c is shown with increasing primary wave frequency. With the primary wave groups selected for the present study, wave groups with the largest mean frequency have the highest group frequency. The offshore directed low-frequency wave at the still water shoreline mainly comprised the low-frequency wave reflected from the beach. Long wave reflection from the beach is highest at the lowest group frequency and therefore gives the largest radiation coefficient.

5. Conclusions

A phase resolving Boussinesq type numerical wave model is used to investigate low-frequency waves in the surf and swash zones of various sea bottom slopes. Numerical simulations of surface elevations of both primary waves and low-frequency waves across the surf zone were first compared with experimental data and good agreement found. A series of numerical experiments were then performed to derive low-frequency waves generated from fully modulated bichromatic waves propagating on various sea bottom slopes. Low-frequency wave characteristics are then discussed in terms of their physical nature and the relationship to the primary wave field on a series of sea bottom slopes.

Unlike primary waves, low-frequency wave energy increases across the surf zone and on certain occasions low-frequency waves as high as 12 times its offshore counterpart were found at the still water shoreline. Gentle beach slopes in general gave the largest amplification of low-frequency waves across the surf zone. On gentle slopes, the time-varying breakpoint generated low-frequency waves which dominate the energy in the low-frequency band due to high intensity of wave breaking and the

presence of a wide surf zone. At the still water shoreline of the 1:30 beach, the height of the low-frequency wave was 2.6 times that of the local primary waves at the mean frequency of 0.8 Hz and was more than 1.4 at its lowest. On steep beaches, where the surf zone is only partially saturated, low-frequency wave height at the still water shoreline varied between 0.5 and 1.0 times that of local primary waves.

Swash fluctuations on mild slopes are predominantly driven by wave energy at the group frequency. On steep slopes, a significant proportion of short wave energy contributes to drive swash motions and individual swash events driven by short waves become more significant. The low-frequency component of the swash excursion reduces with an increase in bottom slope irrespective of the mean frequency of the incident wave groups.

Low-frequency wave radiation from the surf zone on a given beach slope depends on the mean frequency of the primary waves. Higher primary frequencies which lead to wider surf zones tend to radiate more low-frequency wave energy in the offshore direction. No apparent relationship is observed between the radiation of low-frequency waves and the surf similarity parameter which primarily indicates the complex relationship of low-frequency waves with incident waves and bottom bathymetry.

Swash motions and low-frequency water surface fluctuations predominantly drive sediments on steep beach slopes. Therefore, the results found in this research will be very useful in studying morphodynamics of the surf and swash zones and hence planning and design of shore protection schemes.

Acknowledgement

The authors are very grateful to Prof. Hajime Mase and Dr. Tom Baldock for providing high quality data sets for the validation of the numerical model.

References

- Baldock, T.E., Huntley, D.A., 2002. Long wave forcing by the breaking of random gravity waves on a beach. *Proceedings of the Royal Society of London* 458, 2177–2201.
- Baldock, T.E., Simmonds, D.J., 1999. Separation of incident and reflected waves over sloping bathymetry. *Coastal Engineering* 38, 167–176.
- Baldock, T.E., Holmes, P., Horn, D.P., 1997. Low frequency swash motion induced by wave grouping. *Coastal Engineering* 32, 197–222.
- Baldock, T.E., Huntley, D.A., Bird, P.A.D., O'Hare, T., Bullock, G.N., 1999. Breakpoint generated surf beat induced by bichromatic wave groups. *Coastal Engineering* 39, 213–242.
- Guza, R.T., Thornton, E.B., 1985. Observations of surf beat. *Journal of Geophysical Research* 90, 3162–3172.
- Huntley, D.A., Guza, R.T., Thornton, E.B., 1981. Field observations of surf beat I. Progressive edge waves. *Journal of Geophysical Research* 86, 6451–6466.
- Karunarathna, H., Tanimoto, K., 1995. Numerical experiments on low-frequency fluctuations on a submerged coastal shelf. *Coastal Engineering* 26, 271–289.
- Karunarathna, H., Tanimoto, K., 1996. Long period water surface fluctuations on a horizontal coastal shelf with a steep seaward face. *Coastal Engineering* 29, 123–147.
- Karunarathna, H., Chadwick, A.J., Lawrence, J., 2005. Numerical experiments of swash oscillations on steep and gentle beaches. *Coastal Engineering* 52, 457–511.
- Kennedy, A.B., Chen, Q., Kirby, J., Dalrymple, R., 2000. Boussinesq modelling of wave transformation, breaking and runup, I:1D. *Journal of Waterway, Port, Coastal and Ocean Engineering* 126 (1), 39–47.
- List, J.H., 1991. Wave groupiness variation in the nearshore. *Coastal Engineering* 15, 475–496.
- Louquet-Higgins, M.S., Stewart, R.W., 1962. Radiation stress and mass transport in gravity waves, with application to 'surf beats'. *Journal of Fluid Mechanics* 13, 481–504.
- Louquet-Higgins, M.S., Stewart, R.W., 1964. Radiation stress in water waves: a physical discussion with applications. *Deep Sea Research* 11, 529–562.
- Madsen, P.A., Murray, R., Sørensen, O.R., 1991. A new form of Boussinesq equations with improved linear dispersion characteristics. *Coastal Engineering* 15, 371–388.
- Madsen, P.A., Sørensen, O.R., Schäffer, H.A., 1997a. Surf zone dynamics simulated by a Boussinesq type model. Part I: model description and cross-shore motion of regular waves. *Coastal Engineering* 32, 255–287.
- Madsen, P.A., Sørensen, O.R., Schäffer, H.A., 1997b. Surf zone dynamics simulated by a Boussinesq type model. Part II: surf beat and swash oscillations for wave groups and irregular waves. *Coastal Engineering* 32, 289–319.
- Mase, H., 1994. Uprush-backrush interaction dominated and long wave dominated swash oscillations. In: *Proceedings of International Symposium: Waves-Physical and Numerical Modelling*, Vancouver, Canada, pp. 316–325.
- Mase, H., 1995. Frequency downshift of swash oscillations compared to incident waves. *Journal of Hydraulic Research* 33 (3), 397–411.
- Munk, W.H., 1949. Surf beats. *Transactions—American Geophysical Union* 30, 849–854.
- Schäffer, H.A., 1993. Infragravity waves forced by short wave groups. *Journal of Fluid Mechanics* 247, 551–588.
- Symonds, G., Huntley, D.A., Bowen, A.J., 1982. Two dimensional surf beat: long wave generation by a time-varying break point. *Journal of Geophysical Research* 87, 492–498.
- Tucker, M.J., 1950. Surf beats: sea waves of 1 to 5 min period. *Proceedings of the Royal Society London A* 202, 565–573.